JACS
JOURNAL OF THE AMERICAN CHEMICAL SOCIETY
Article
pubs.acs.org/JACS

Necroptosis-Inducing Rhenium(V) Oxo Complexes

Kogularamanan Suntharalingam,[†,§] Samuel G. Awuah,[†] Peter M. Bruno,[‡] Timothy C. Johnstone,[†] Fang Wang,[†] Wei Lin,[†] Yao-Rong Zheng,[†] Julia E. Page,[†] Michael T. Hemann,[‡] and Stephen J. Lippard*[,†,‡]

[†]Department of Chemistry, Massachusetts Institute of Technology, Cambridge, Massachusetts 02139, United States

[‡]The Koch Institute for Integrative Cancer Research, Massachusetts Institute of Technology, Cambridge, Massachusetts 02139, United States

[§]Department of Chemistry, King's College London, London SE1 1DB, United Kingdom

Supporting Information

ABSTRACT: Rhenium(V) oxo complexes of general formula $[ReO(OMe)(N^N)Cl_2]$, where N^N = 4,7-diphenyl-1,10-phenanthroline, **1**, or 3,4,7,8-tetramethyl-1,10-phenanthroline, **2**, effectively kill cancer cells by triggering necroptosis, a non-apoptotic form of cell death. Both complexes evoke necrosome (RIP1-RIP3)-dependent intracellular reactive oxygen species (ROS) production and propidium iodide uptake. The complexes also induce mitochondrial membrane potential depletion, a possible downstream effect of ROS production. Apparently, **1** and **2** are the first rhenium complexes to evoke cellular events consistent with programmed necrosis in cancer cells. Furthermore, **1** and **2** display low acute toxicity in C57BL/6 mice and reasonable stability in fresh human blood.

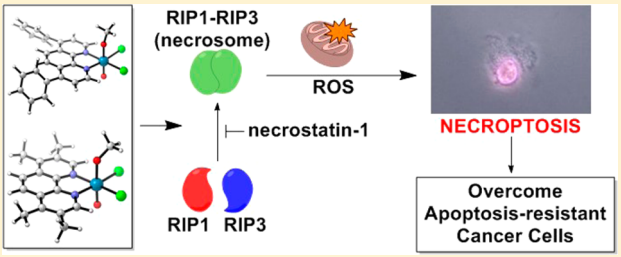

INTRODUCTION

Cancer is a leading cause of death and suffering throughout the world and continues to impose a huge socio-economic burden on society. According to the latest statistics released by the World Health Organization, an estimated 8.2 million cancer-related deaths occurred in 2012, a 0.6 million increase from the previous estimation in 2008.[1] With the global cancer burden rising, the development of new cancer treatments is crucial. Since the discovery of their antineoplastic properties in 1969, platinum drugs such as cisplatin, oxaliplatin, and carboplatin have become a mainstay chemotherapy for cancer.[2,3] Their use, however, is limited by side effects and inherent or acquired resistance.[4−6] These limitations have driven the search for new treatments, including investigations of other transition metal compounds. Many ruthenium, osmium, titanium, copper, iron, and other metal compounds have been tested for their anticancer activity, and some of the most promising candidates have been studied clinically.[7]

Several rhenium-based compounds have been employed as in vitro and in vivo imaging agents, but in-depth studies exploring their antiproliferative properties are relatively rare.[8,9] The most active rhenium compounds reported to date contain Re(I) carbonyl centers bound to mono-, di-, or tridentate ligands.[10−14] This class of compounds are proposed to induce their cytotoxic effects through covalent interactions with DNA bases and/or protein side chains. A number of photolabile rhenium(I) derivatives that trigger cell death upon irradiation have also been devised.[15−17] These complexes offer temporal and spatial control over activation and therefore could be useful in overcoming systemic toxicity. Recently, octahedral Re(IV) complexes bearing polypyridyl ligands were discovered to exhibit potent in vitro antiproliferative activity against breast, ovarian, and prostate cancer cells.[18] The complexes were hypothesized to interact with nuclear DNA upon hydrolysis, inducing apoptotic cell death. The anticancer potential of dinuclear rhenium compounds has also been investigated.[19−21] In addition to displaying promising anticancer activity, paddle-wheel dirhenate(III) complexes have attractive pharmacological features such as low neuro-, hepato-, and nephrotoxicity.[21−24] Dirhenate(III) units with propionate ligands and quadruple Re−Re bonds have varying degrees of efficacy in sarcoma-, leukemia-, and melanoma-bearing mice models.[25] Subsequent studies found that the anticancer activity of the rhenium clusters depends on the identity and orientation of the ligands around the two rhenium(III) centers rather than the presence of a quadruple bond. Remarkably, dinuclear rhenium(III) analogues bearing alkylcarboxylates and zwitterionic aminocarboxylate ligands inhibited tumor growth by up to 60% in Wistar rats inoculated with tumor carcinoma Guerink (T8) cells. Furthermore, when combined with cisplatin, the rhenium(III) clusters completely inhibited tumor progression.[21−24,26] Dirhenate(III) complexes are also regarded as promising modulators of cisplatin. According to in vitro and in vivo studies, carboxylate-bridged dirhenate(III) complexes stabilized red blood cells against hemolysis, thereby

Received: November 23, 2014
Published: February 20, 2015

DOI: 10.1021/ja511978y
J. Am. Chem. Soc. 2015, 137, 2967−2974

diminishing the dose-limiting toxicity associated with cisplatin.[21−24,27]

Many clinically used anticancer agents act by targeting and damaging nuclear DNA, eventually leading to apoptosis.[28−31] Cytotoxic compounds may also kill cells through non-apoptotic cell death pathways such as necrosis.[32−34] Although necrosis was previously believed to be a random, unregulated process, it is now understood that programmed necrosis, also known as necroptosis, does occur in certain cell types.[35] Necroptosis also plays a role in inflammation.[36] Necroptosis is activated by the formation of a complex between receptor-interacting protein (RIP) kinases, RIP1 and RIP3.[37] The RIP1-RIP3 complex, also known as a necrosome, is thought to modulate oxidative stress and generate mitochondrial reactive oxygen species (ROS) capable of inducing bioenergetics-related cell death.[38] The relationship between ROS production and necroptotic cell death is poorly understood, although some reports link RIP1 and ROS-induced cell death.[39] Owing to the prevalence of apoptosis-inducing anticancer drugs, resistance to apoptosis has been observed in many cancers.[40−42] Therefore, chemotherapies capable of inducing non-apoptotic cell death such as necroptosis warrant further investigation. Here we present the synthesis, characterization, and cell-based studies of two necroptosis-inducing rhenium(V) oxo complexes.

RESULTS AND DISCUSSION

Synthesis and Characterization. The rhenium(V) oxo complexes **1** and **2** were prepared by the reaction of $[ReOCl_3(PPh_3)_2]$ with 1.5 equiv of the corresponding bidentate ligand in methanol (Scheme 1). The complexes were isolated in reasonable yields as pale green solids and fully characterized by NMR and IR spectroscopy and ESI mass spectrometry. The purity of the complexes was confirmed by elemental analysis. Variable-temperature ^{1}H NMR spectroscopic studies in dimethylsulfoxide (DMSO) revealed the complexes to be stable and to remain intact at elevated temperatures (up to 75 °C, see Figure S1).

Scheme 1. Reaction Scheme for Preparing Rhenium(V) Oxo Complexes, 1 and 2

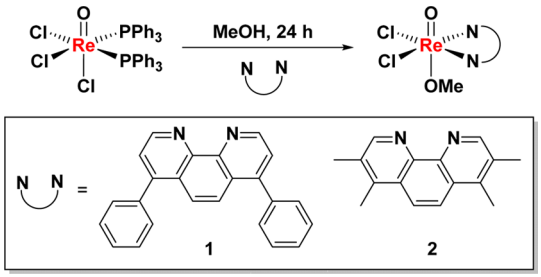

The lipophilicity of the rhenium(V) oxo complexes, **1** and **2**, was determined by measuring the extent to which they partition between octanol and water, $P_{o/w}$ or P. The experimentally determined log P values are 1.20 for **1**, and 0.95 for **2**. The hydrophobic character of the rhenium(V) oxo complexes suggests that they will be taken up well by cells.

In Vitro Potency. The in vitro effect of rhenium(V) oxo complexes **1** and **2** toward a panel of human cell lines was determined by the colorimetric MTT [3-(4,5-dimethylthiazol-2-yl)-2,5-diphenyltetrazolium bromide] assay. Cisplatin was also included as a control. The IC_{50} values, or concentration required to induce 50% cell death, were derived from dose−response curves and are summarized in Table 1. In cancer cells, the IC_{50} values of **1** and **2** are in the sub-micromolar range, whereas in normal fibroblast cells, the IC_{50} values of **1** and **2** are in the micromolar range (about 10-fold higher). The potency of the rhenium complexes was significantly higher than that of cisplatin for the cell lines tested. Notably, the IC_{50} value of **2** is 20 times lower in lung carcinoma A549 cells than the IC_{50} value of cisplatin. The high potency observed for **1** and **2** can, in part, be attributed to their inherent lipophilic character (log P = 1.20 for **1**, and 0.95 for **2**). Indeed, the IC_{50} values of cytotoxic platinum complexes of comparable lipophilicity are similar to those observed for **1** and **2** in HeLa cervical adenocarcinoma cells.[43] Specifically, the IC_{50} values in HeLa cervical adenocarcinoma cells of ester-bearing bis(carboxylato)dichlorido(ethane-1,2-diamine)platinum(IV) complexes with log P values of 0.70 and 1.69 are 110 nM and 32 nM, respectively.[44] Furthermore, the rhenium complexes are not cross-resistant with cisplatin, as demonstrated by their ability to kill cisplatin-resistant ovarian carcinoma cells (A2780CP70) with up to 15 times greater potency than cisplatin-sensitive cells (A2780).

Given the ability of **1** and **2** to selectively kill ovarian cisplatin-resistant cells over the corresponding cisplatin-sensitive cells, we evaluated their potency against other cisplatin-resistant cell lines such as HT-29 (colorectal adenocarcinoma), MDA-MB-231 (breast adenocarcinoma), PC-3 (prostate adenocarcinoma), MCF-7 (breast adenocarcinoma), and DU 145 (prostate carcinoma). The rhenium complexes displayed nanomolar and sub-micromolar toxicities toward the cisplatin-resistant cells (Table 2). Remarkably, the IC_{50} values for **1** and **2** are 300-fold lower in colorectal adenocarcinoma HT-29 cells than the IC_{50} value of cisplatin. Although cisplatin is one of the most successful broad-spectrum anticancer drugs in clinical use, several tumors exhibit resistance. A plethora of molecular mechanisms account for cisplatin resistance, including reduced intracellular accumulation, increased sequestration by scavengers, efficient DNA repair, and deregulation of proteins involved in the DNA damage

Table 1. IC_{50} Values (nM) of 1, 2, and Cisplatin against Various Cancerous and Healthy Cell Lines after 72 h Exposure[a]

cell line	cancer type	1	2	cisplatin
A549	lung carcinoma	207 ± 4	157 ± 15	3230 ± 467
HeLa	cervical adenocarcinoma	445 ± 4	695 ± 21	4100 ± 113
U2OS	bone osteosarcoma	274 ± 6	209 ± 31	4600 ± 600[b]
NTERA-2	testis carcinoma	230 ± 28	255 ± 35	385 ± 49
A2780	ovarian carcinoma	670 ± 40	150 ± 10	700 ± 200[b]
A2780CP70	ovarian carcinoma	42 ± 15	56 ± 2	8415 ± 205
MRC-5	lung fibroblast	1351 ± 228	709 ± 76	5300 ± 600[b]

[a]The errors represent standard deviations. [b]IC_{50} values taken from ref 45.

DOI: 10.1021/ja511978y
J. Am. Chem. Soc. 2015, 137, 2967−2974

Table 2. IC_{50} Values (nM) of 1, 2, and Cisplatin against a Panel of Cisplatin-Resistant Cell Lines and Confluent Lung Carcinoma A549 Cells after 72 h Exposure[a]

cell line	cancer type	1	2	cisplatin
HT-29	colorectal adenocarcinoma	85 ± 11	95 ± 20	29640 ± 1329
MDA-MB-231	breast adenocarcinoma	475 ± 161	1735 ± 275	43600 ± 7071
MCF-7	breast adenocarcinoma	285 ± 35	805 ± 21	9740 ± 537
PC-3	prostate adenocarcinoma	270 ± 14	780 ± 10	10250 ± 919
DU 145	prostate carcinoma	2840 ± 381	1370 ± 84	>100000
A549 (confluent)	lung carcinoma	8610 ± 749	5245 ± 1986	9420 ± 1937

[a]The errors represent standard deviations.

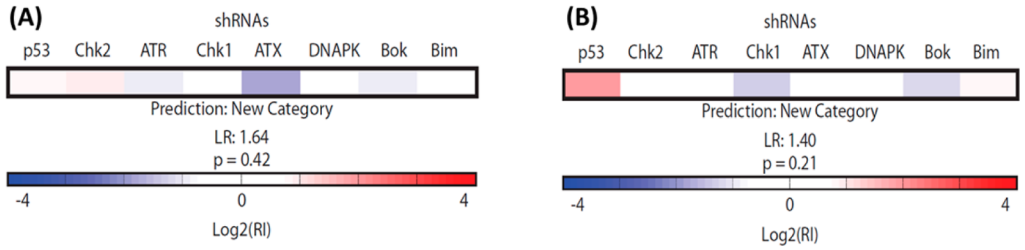

Figure 1. RNAi signatures derived from the treatment of Eμ-Myc$^{p19arf-/-}$ lymphoma cells with **1** (A) and **2** (B) at the LD80−90 (1 μM) concentration for each compound. The exposure time was 72 h.

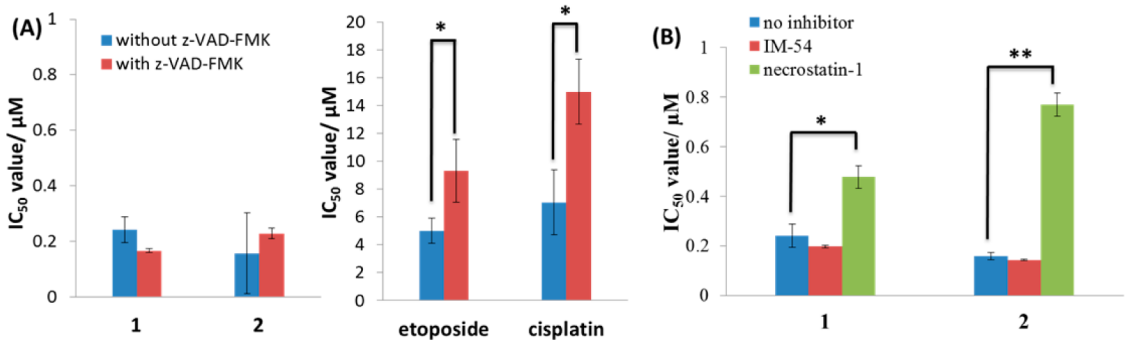

Figure 2. (A) IC_{50} values (in μM) of **1**, **2**, etoposide, and cisplatin against A549 cells in the absence and presence of apoptosis inhibitor, z-VAD-FMK (5 μM), after 72 h incubation. (B) IC_{50} values (in μM) of **1** and **2** against A549 cells in the absence and presence of H_2O_2-induced necrosis inhibitor, IM-54 (10 μM), and necroptosis inhibitor, necrostatin-1 (60 μM), after 72 h incubation. Student's t test, $p < 0.05$ or 0.01. Error bars represent standard deviations.

and apoptotic cell death pathways.[46] Therefore, compounds such as **1** and **2**, which can overcome cisplatin resistance, hold significant therapeutic potential. To further investigate this potential, cytotoxicity studies were conducted with confluent A549 cells (Table 2). The IC_{50} values for **1** and **2** are 40-fold higher in confluent A549 cells than in A549 cells in log phase growth. This result highlights the ability of **1** and **2** to selectively kill fast-growing cancer cells.

Cellular Mechanism of Action and Mode of Cell Death. To gain insight into how the rhenium complexes induce cell death, **1** and **2** were analyzed by a recently developed functional strategy employing a RNAi signature assay to predict the mechanism of cytotoxic drug action.[47−49] This RNAi-based methodology relies on a fluorescence competition assay with lymphoma cells that are partially infected with eight distinct short hairpin RNAs (shRNAs). shRNA-bearing cells will either enrich or deplete relative to the uninfected population based on the survival advantage or disadvantage conferred by a given shRNA. The responses of these cells compose signatures, which have been obtained from all classes of clinically used cytotoxic agents. These signatures comprise a reference set which is then informatically classified by a probabilistic K-nearest neighbors algorithm to determine whether a new compound belongs to a class in the reference set or requires a new category not yet represented. Neither **1** nor **2** classified as belonging to any category of drug mechanism present in the reference set, and thus they represent novel mechanisms of drug action (Figure 1).

In order to determine the cell-killing mechanism of **1** and **2**, we carried out cytotoxicity studies in the presence of apoptosis and necrosis inhibitors. Upon addition of z-VAD-FMK, a potent inhibitor of caspase-mediated apoptosis,[50] the ability of **1** and **2** to kill A549 cells remained largely unaltered, indicative of a non-apoptotic cell death program (Figure 2A). By contrast, the IC_{50} values for known apoptosis-inducing agents such as etoposide and cisplatin increased significantly (t test, $p < 0.05$) in the presence of the inhibitor (Figure 2A). Immunoblotting studies showed that proteins implicated in the apoptotic cell death pathway, namely, cleaved caspases 7 and 9, were not detected in **1**- and **2**-treated A549 cells (50−500 nM for 72 h; Figure S2), providing further evidence for a non-apoptotic program. We next investigated the possibility that **1** and **2** induce necroptosis. Necroptosis is a well-regulated mode of cell death that is different from unregulated necrosis and apoptosis.[35] Unlike unregulated necrosis, which can be induced by H_2O_2 or heat, necroptosis

DOI: 10.1021/ja511978y
J. Am. Chem. Soc. 2015, 137, 2967−2974

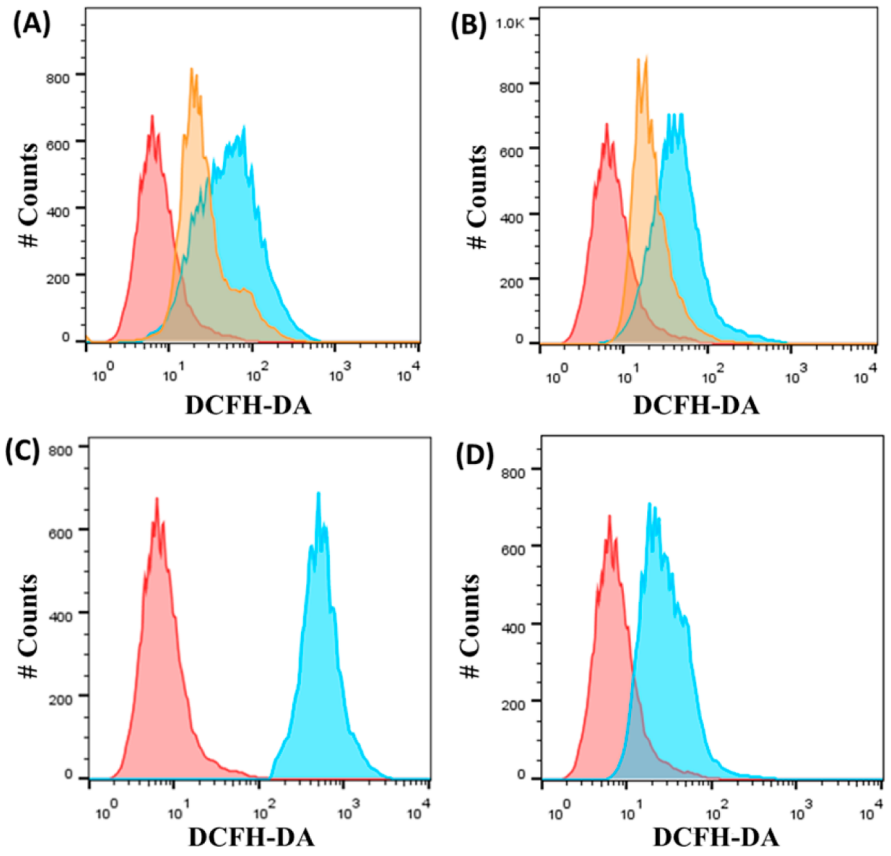

Figure 3. (A) Representative histograms displaying the green fluorescence emitted by DCFH-DA-stained A549 cells (red) and A549 cells treated with **1** (20 μM for 12 h) (blue) or **1** (20 μM for 12 h) with nectrostatin-1 (60 μM for 12 h) (orange). (B) Representative histograms displaying the green fluorescence emitted by DCFH-DA-stained A549 cells (red) and A549 cells treated with **2** (20 μM for 12 h) (blue) or **2** (20 μM for 12 h) with nectrostatin-1 (60 μM for 12 h) (orange). (C) Representative histograms displaying the green fluorescence emitted by DCFH-DA-stained A549 cells (red) and A549 cells treated with H_2O_2 (1 mM for 1 h) (blue). (D) Representative histograms displaying the green fluorescence emitted by DCFH-DA-stained A549 cells (red) and A549 cells treated with shikonin (20 μM for 12 h) (blue).

relies on the interaction of protein kinases, RIP1 and RIP3, to initiate cell disintegration. This process can be blocked by necrostatin-1, a potent RIP1 kinase inhibitor.[51,52] To determine whether **1** and **2** induced necroptosis and/or uncontrolled necrosis, cytotoxicity studies were conducted in the presence of necrostatin-1 (60 μM) and IM-54 (10 μM), an inhibitor of H_2O_2-induced necrosis.[53] Co-incubation with necrostatin-1 markedly decreased the toxicity of **1** and **2** (t test, $p < 0.05$) against A549, PC-3, and HT-29 cells (Figures 2B and S3). A similar effect was also observed for shikonin, a naturally occurring compound known to induce necroptosis in certain cell types (Figure S3A).[39] In contrast, co-treatment with IM-54 did not significantly affect the toxicity of **1** and **2** (Figure 2B). Taken together, the cytotoxicity data suggest that **1** and **2** induce RIP1-RIP3 (necrosome)-mediated necroptosis, rather than uncontrolled necrosis or apoptosis. Immunoblotting studies revealed that the overall expression level of RIP1 and RIP3 in A549 cells remained unchanged with increasing **1** and **2** dosages (Figure S2). Therefore, **1**- and **2**-induced cell death relies on RIP1-RIP3 complex formation and not on the expression levels of the individual protein kinases. RIP1 can also form a cytosolic complex with Fas-associated death domain (FADD) and caspase 8, known as a ripoptosome, to initiate apoptosis (through caspase 8 cleavage).[54−56] Immunoblotting studies showed that FADD and cleaved caspase 8 expression remained unaltered with increasing **1** and **2** concentration (Figure S2), indicating that ripoptosome formation was not responsible for **1**- and **2**-induced cell death. This is consistent with the fact that **1**- and **2**-treated A549 cells do not undergo apoptosis.

Characterization of Necroptotic Features. Having established that necrosome formation is a determinant of **1** and **2** activity, we performed additional studies to understand the cascade of events leading from necrosome formation to cell death. Necrosomes generate abnormally high levels of mitochondrial ROS,[57−59] leading to ATP depletion and eventual degradation of the mitochondrial membrane potential.[60,61] With this fact in mind, we quantified intracellular ROS production by flow cytometry using 6-carboxy-2′,7′-dichlorodihydrofluorescein diacetate (DCFH-DA), a well-established ROS indicator. A549 cells incubated with **1** and **2** (20 μM for 12 h) displayed markedly higher levels of ROS than untreated control cells (Figure 3A,B). A549 cells dosed with H_2O_2 (1 mM for 1 h, ROS-inducer) and shikonin (20 μM for 12 h, necroptosis-inducer) also exhibited significantly higher levels of measurable ROS than untreated cells (Figure 3C,D). Remarkably, **1**- and **2**-induced ROS production was attenuated in the presence of necrostatin-1 (60 μM) (Figure 3A,B), suggesting that the RIP1-RIP3 kinase complex plays a role in modulating intracellular ROS production.

The effect of **1** and **2** on the mitochondrial membrane potential was assessed by flow cytometry, using the JC-1 assay (5,5′,6,6′-tetrachloro-1,1′,3,3′-tetraethylbenzimidazolyl carbocyanine iodide).[62,63] JC-1 is a cationic lipophilic dye that localizes in the mitochondria of healthy cells as red-emitting aggregates. If the mitochondrial membrane potential is

DOI: 10.1021/ja511978y
J. Am. Chem. Soc. 2015, 137, 2967−2974

disrupted, JC-1 forms green-emitting monomers. A549 cells incubated with **1** and **2** (20 μM for 12 h) displayed increased green fluorescence compared to untreated cells, indicative of mitochondrial membrane disruption (Figure S4A,B). A similar result was observed for A549 cells dosed with carbonyl cyanide *m*-chlorophenyl hydrazone (CCCP) (5 μM for 12 h), a known mitochondrial membrane depolarizer (Figure S4C), and shikonin (20 μM for 12 h), a necroptosis-inducing agent (Figure S4D). Notably, **1**- and **2**-induced mitochondrial membrane depletion was amplified with necrostatin-1, suggesting that **1** and **2** may inherently target mitochondria and induce mitochondrial dysfunction, independent of RIP1-RIP3 formation. This could explain the high residual toxicity (>1 μM) observed for A549 cells co-incubated with the rhenium complexes (**1** and **2**) and necrostatin-1 (Figure 2B).

Intracellular ROS production and mitochondrial membrane depletion contribute to necroptosis.[60,61] Cells undergoing necroptosis display necrosis-like morphological features such as loss of cell membrane integrity, increase in organelle and cell volume (oncosis), and intact nuclear membrane.[64−66] To further test whether **1**- and **2**-treatment is able to trigger necroptosis, Hoechst 33258/propidium iodide (PI) double staining was carried out to determine nuclear membrane morphology and integrity. Hoechst 33258 is a DNA minor groove binder that is routinely used to visualize the nucleus without the need for cell permeabilization.[67] When used without cell permeabilization agents, PI stains the nuclei of necrotic cells.[68] Early-stage apoptotic and normal cells maintain cell membrane integrity and thus are not stained by PI. A549 cells were treated with **1** and **2** (20 μM for 12 h), incubated with Hoechst 33258 and PI, and imaged using a fluorescence microscope. Untreated A549 cells exhibited bright blue nuclei, owing to Hoechst 33258 uptake (Figure 4A). Cells incubated with **1** and **2** displayed pink nuclei,

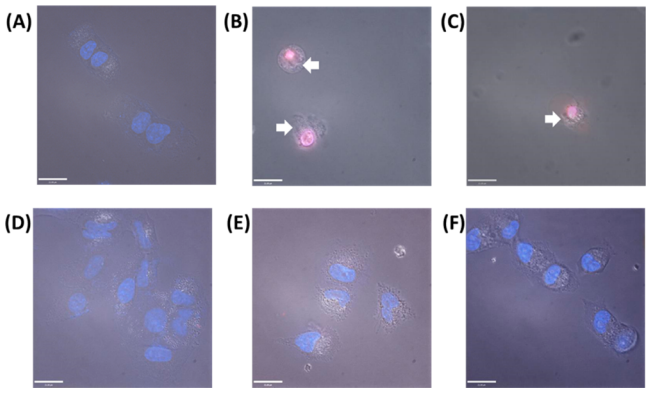

Figure 4. Fluorescence microscopy images of A549 cells untreated (A) and treated with **1** (20 μM for 12 h) (B), **2** (20 μM for 12 h) (C), necrostatin-1 (60 μM for 12 h) (D), **1** and necrostatin-1 (E), and **2** and necrostatin-1 (F) and then stained with Hoechst 33258 and PI. Arrows indicate signs of cell membrane disintegration. Scale bar = 21 μM.

owing to Hoechst 33258 and PI uptake, which is consistent with necroptosis (Figure 4B,C). Furthermore, **1**- and **2**-treated cells showed clear signs of plasma membrane disintegration with undamaged nuclei. A549 cells co-incubated with **1** or **2** and necrostatin-1 (60 μM for 12 h) were unstained by PI, suggesting that necrostatin-1 is able to block **1**- and **2**-induced necroptosis (Figure 4E,F). Overall, the microscopy data suggest that necrosome formation contributes to the necrosis-like morphological features observed upon treatment with **1** and **2**. To further validate this result, A549 cells were treated under the same conditions as above, stained with PI, and analyzed by flow cytometry. Complementary to the microscopy results, **1**- and **2**-treated cells exhibited higher PI uptake compared to untreated control cells, indicative of necrotic cell death (Figure S5A,B). The flow cytometry data also showed that necrostatin-1 could block **1**- and **2**-mediated PI uptake. Additional studies showed that pretreatment of A549 cells with *N*-acetylcysteine (3 mM for 1 h), a ROS inhibitor, significantly decreased **1**- and **2**-induced PI uptake (Figure S5C,D). This result suggests that intracellular ROS generation is an integral part of the necroptotic mechanism of action of **1** and **2**.

PARP-1- and p53-Independent Necroptosis. Apart from necrosome formation, necroptosis can also result from the overactivation of poly(ADP−ribose) polymerase (PARP-1).[65,66] PARP-1 is a nuclear enzyme that is involved in DNA repair and transcriptional regulation.[69] DNA damage can trigger PARP-1 activity, resulting in ATP and NAD depletion and bioenergetics-mediated cell death.[70] To determine whether PARP-1 activity is a factor in **1**- and **2**-mediated cell death, cytotoxicity assays were conducted with wild-type mouse embryonic fibroblast cells (MEFs PARP-1$^{+/+}$) and the corresponding PARP-1-null cells (MEFs PARP-1$^{-/-}$). The IC_{50} values for **1** and **2** were similar for MEFs PARP-1$^{+/+}$ and MEFs PARP-1$^{-/-}$ cells, indicating that **1**- and **2**-induced necroptosis is independent of PARP-1 function (Figure 5A). This result is consistent with immunoblotting studies, which revealed that treatment with **1** and **2** did not up-regulate canonical markers of DNA damage, such as the phosphorylated forms of H2AX (γH2AX) and CHK2 (Figure S6). Recently, p53 has also been reported to play a role in necroptosis. p53 induces cathepsin Q, a lysosomal protease that cooperates with ROS to execute necrosis.[71] To investigate whether p53 might play a role in **1**- and **2**-mediated necroptosis, cytotoxicity studies were conducted with HCT116 p53$^{+/+}$ and HCT116 p53$^{-/-}$ cells. The potency of **1** and **2** was statistically similar for HCT116 p53$^{+/+}$ and HCT116 p53$^{-/-}$ cells, indicating that **1** and **2** induce necroptosis in a manner that is independent of p53 (Figure 5B). This conclusion is consistent with the RNAi signatures, which revealed that p53 is not important in the cellular response evoked by the complexes, especially for **1**. Apart from the implications of this result for the mechanism of action of **1** and **2**, it is clinically very appealing because p53 is mutated, defective, or inactivated in several chemoresistant cancers.

Cell Cycle Analysis. To gain a more complete understanding of the cellular response evoked, DNA-flow cytometric studies were conducted to determine the effect of **1** and **2** on the cell cycle. A549 cells were treated with **1** or **2** (2 μM), and the cell cycle was determined over the course of 72 h (Figure S7). After 24 h treatment, both complexes stalled the cell cycle at the G1 phase. Cells treated with **1** remained stalled at the G1 phase after 48 h. Upon further incubation (72 h), large populations of cell debris were detected (32%), indicative of cell death. Cells incubated with **2** for 48 and 72 h also displayed large populations of debris (26% and 38%, respectively). G1-phase cell cycle arrest followed by immediate cell death is characteristic of programmed necrosis.[72,73]

In Vivo Toxicity and Stability in Whole Human Blood. Given the impressive in vitro data acquired for **1** and **2**, an in vivo study was conducted with C57BL/6 mice to determine acute toxicity and possible side effects. Single doses of **1** and **2** (3, 7, 11, 15, 20, and 36 mg/kg) in saline were administered by intraperitoneal injection. The mice were then monitored for signs of pain, distress, and weight loss for 6 days post-treatment.

DOI: 10.1021/ja511978y
J. Am. Chem. Soc. 2015, 137, 2967−2974

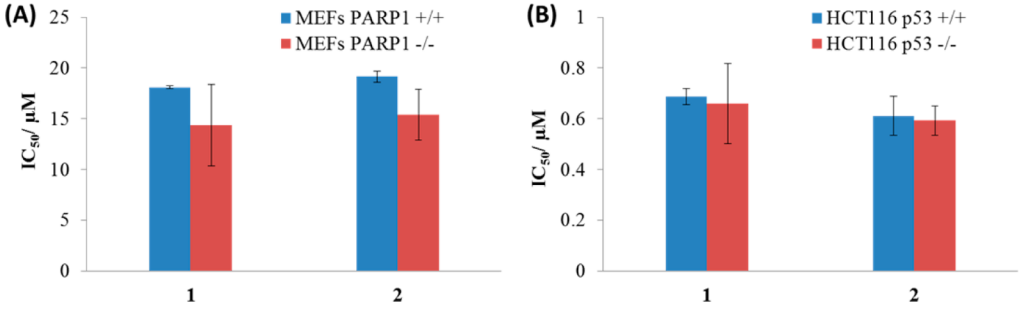

Figure 5. (A) IC_{50} values (in μM) of **1** and **2** against MEFs PARP-$1^{+/+}$ and MEFs PARP-$1^{-/-}$ cells after 72 h incubation. (B) IC_{50} values (in μM) of **1** and **2** against HCT116 $p53^{+/+}$ and HCT116 $p53^{-/-}$ cells after 72 h incubation.

The compounds exhibited no toxicity in mice, as gauged by a lack of weight loss after treatment. The change in weight of mice after a single dose of **1** and **2** at the maximum solubility of the complexes (36 mg/kg) is depicted in Figure S8. A single 30 mg/kg dose of cisplatin induces acute nephrotoxicity in C57BL/6 mice.[74] The in vivo data highlight the relatively low toxicity of **1** and **2** compared to cisplatin in C57BL/6 mice. The pharmacological toxicity profile of **1** and **2** is very appealing in terms of further preclinical studies.

The stability of biologically active compounds in human blood is vitally important for their potential application in clinical settings. We therefore investigated the stability of **1** in whole human blood using a recently developed protocol.[75] This method exploits the ability of octanol to extract hydrophobic metal complexes such as **1**. The rhenium complex **1** (500 μM) was incubated with fresh human blood at 37 °C, and aliquots were extracted into octanol at various time points. The amount of **1** in the octanol extracts (corresponding to unreacted **1**) was measured by graphite furnace atomic absorption spectroscopy (GFAAS). The data presented in Figure S9 revealed that the half-life of **1** in human blood is 29.1 min, comparable to that reported for cisplatin ($t_{1/2}$ = 21.6 min).[76]

CONCLUSION

Two rhenium(V) oxo complexes were prepared, and their in vitro properties were investigated. The complexes selectively kill cancer cells over normal cells and display markedly higher cell toxicity than cisplatin. Remarkably, the IC_{50} values of **1** and **2** are 2 orders of magnitude lower in colorectal adenocarcinoma cells than the IC_{50} value of cisplatin. Cells treated with **1** and **2** displayed features consistent with programmed necrosis (necroptosis), including RIP1-RIP3-dependent intracellular ROS production, cell membrane disruption, PI uptake, mitochondrial damage, and G1 cell cycle arrest. Given the inherent and/or acquired resistance of tumors toward apoptosis-inducing chemotherapies, compounds such as **1** and **2**, capable of killing cancer cells through necroptosis, are highly sought-after when selecting preclinical drug candidates for chemoresistant malignancies.

EXPERIMENTAL DETAILS

Material. All synthetic procedures were performed under normal atmospheric conditions without exclusion of oxygen or moisture. The bidentate aromatic ligands 4,7-diphenyl-1,10-phenanthroline and 3,4,7,8-tetramethyl-1,10-phenanthroline were purchased from Sigma-Aldrich and used as received. $ReOCl_3(PPh_3)_2$ was prepared as previously reported.[77] The synthesis of **1** has been reported previously,[78] but the procedure reported here is novel. Analytical-grade acetone and dichloromethane were used as solvents.

Physical Measurements. NMR measurements were recorded on a Bruker 400 MHz spectrometer in the MIT Department of Chemistry Instrumentation Facility (DCIF) at 20 °C. ^{1}H and $^{13}C\{^1H\}$ NMR chemical shifts were referenced internally to residual solvent peaks or relative to tetramethylsilane ($SiMe_4$, δ = 0.00 ppm). Fourier transform infrared (FTIR) spectra were recorded with a ThermoNicolet Avatar 360 spectrophotometer upon preparation of the samples as KBr disks. The spectra were analyzed using the OMNIC software. GFAAS was carried out using a Perkin-Elmer AAnalyst600 spectrometer.

Synthesis of [ReO(OMe)(4,7-diphenyl-1,10-phenanthroline)-Cl_2] (1). $[ReOCl_3(PPh_3)_2]$ (63.8 mg, 0.08 mmol) was suspended in methanol (15 mL) and heated to 50 °C. To this mixture was added a methanolic solution (5 mL) of 7-diphenyl-1,10-phenanthroline (34.0 mg, 0.10 mmol). The resultant mixture was heated under reflux for 24 h to give a deep purple solution with a pale green precipitate. The precipitate was filtered and then washed with hot methanol, cold methanol, and diethyl ether. The rhenium(V) oxo complex was isolated as a pale green solid. Yield: 19.8 mg (37%). Mp 247 °C (dec). ^{1}H NMR (400 MHz, DMSO-d_6): δ 10.08 (d, 2H), 8.48 (d, 2H), 8.31 (s, 2H), 7.83 (m, 4H), 7.73 (m, 6H), 2.56 (s, 3H). IR (KBr, cm^{-1}): 941.51 (Re═O), 508.42 (Re-OMe). ESI-MS (MeOH/DMSO): m/z 605.0 ($[M-OMe]^+$, calcd 605.0). Anal. Calcd for **1**, $C_{25}H_{19}Cl_2N_2O_2Re$: C, 47.17; H, 3.01; N, 4.40. Found: C, 46.79; H, 3.05; N, 4.35.

Synthesis of [ReO(OMe)(3,4,7,8-tetramethyl-1,10-phenanthroline)Cl_2] (2). $[ReOCl_3(PPh_3)_2]$ (50.0 mg, 0.06 mmol) was suspended in methanol (15 mL) and heated to 50 °C. To this mixture was added a methanolic solution (5 mL) of 3,4,7,8-tetramethyl-1,10-phenanthroline (21.85 mg, 0.09 mmol). The resultant mixture was heated under reflux for 24 h to give a deep purple solution with a pale green precipitate. The precipitate was filtered and then washed with hot methanol, cold methanol, and diethyl ether. The rhenium(V) oxo complex was isolated as a pale green solid. Yield: 14.8 mg (41%). Mp >276 °C (gradual darkening and decomposition). ^{1}H NMR (400 MHz, DMSO-d_6): δ 9.69 (s, 2H), 8.60 (s, 2H), 2.99 (s, 6H), 2.74 (s, 6H), 2.36 (s, 3H). IR (KBr, cm^{-1}): 954.85 (Re═O), 492.85 (Re-OMe). ESI-MS (MeOH/DMSO): m/z 509.0 ($[M-OMe]^+$, calcd 509.0). Anal. Calcd for **2**, $C_{17}H_{19}Cl_2N_2O_2Re$: C, 37.78; H, 3.54; N, 5.18. Found: C, 37.76; H, 3.63; N, 4.99.

Cytotoxicity MTT Assay. The colorimetric MTT assay was used to determine the toxicity of **1**, **2**, and cisplatin. Cells (2×10^3 cells/well) were seeded in a 96-well plate. After the cells were incubated overnight, various concentrations of **1**, **2**, and cisplatin (0.3−100 μM) were added and incubated for 72 h (total volume 200 μL). Cisplatin was prepared as a 5 mM solution in phosphate-buffered saline (PBS) and diluted using media. **1** and **2** were prepared as 10 mM solutions in DMSO and diluted using media. The final concentration of DMSO in each well was 0.5%, and this amount was also present in the untreated control. After 72 h, the medium was removed, 200 μL of a 0.4 mg/mL solution of MTT in DMEM, RPMI, or McCoy's 5A was added, and the plate was incubated for an additional 1−2 h. The DMEM/MTT, RPMI/MTT, or McCoy's 5A/MTT mixture was aspirated, and 200 μL of DMSO was added to dissolve the resulting purple formazan crystals. The absorbance of the solution wells was read at 550 nm. Absorbance values were normalized to DMSO-containing control wells and plotted as the concentration of test compound versus % cell viability. IC_{50} values were interpolated from

DOI: 10.1021/ja511978y
J. Am. Chem. Soc. 2015, 137, 2967−2974

the resulting dose-dependent curves. The reported IC_{50} values are the average from at least three independent experiments, each of which consisted of six replicates per concentration level.

For specific cell death inhibitor assays, inhibitors of necroptosis (necrostatin-1, 60 μM), H_2O_2-induced necrosis (IM-54, 10 μM), and apoptosis (v-VAD-FMK, 5 μM) were added to cells and incubated for 1 h prior to treatment with the test compounds.

Reactivity of 1 and 2 with Necrostatin-1. Mixing the rhenium(V) oxo complexes **1** and **2** (20 μM) with necrostatin-1 (60 μM) in DMSO and cell culture media (DMEM, RPMI, and McCoy's 5A) did not result in a precipitate. Incubation of the rhenium(V) oxo complexes **1** and **2** with necrostatin-1 (1:3 ratio) for up to 6 h in DMSO-d_6 did not lead to a chemical reaction, as determined by ^{1}H NMR analysis (Figure S10 and S11). Despite the presence of sulfur and nitrogen atoms in necrostatin-1, the ^{1}H NMR spectra unequivocally prove that the reactivity/bioactivity of **1** and **2** is not compromised by necrostatin-1.

Intracellular ROS Assay. Untreated and treated A549 cells (1.5×10^6 cells/well) grown in six-well plates were incubated with 6-carboxy-2′,7′-dichlorodihydrofluorescein diacetate (20 μM) for 30 min. The cells were then washed with PBS (1 mL × 3), harvested, and analyzed by using a FACSCalibur-HTS flow cytometer (BD Biosciences) (20 000 events per sample were acquired). The FL1 channel was used to assess intracellular ROS levels. Cell populations were analyzed using the FlowJo software (Tree Star).

JC-1 Assay. The JC-1 Mitochondrial Membrane Potential Assay Kit (Cayman) was used. The manufacturer's protocol was followed to carry out this experiment. Briefly, to untreated and treated A549 cells (1.5×10^6 cells/well) grown in six-well plates was added the JC-1 staining solution (100 μL/mL of cell media). The cells were incubated for 30 min, harvested, and analyzed by using the FACSCalibur-HTS flow cytometer (BD Biosciences) (20 000 events per sample were acquired). The FL1 channel was used to assess mitochondrial depolarization. Cell populations were analyzed using the FlowJo software (Tree Star).

Propidium Iodide Uptake. Untreated and treated A549 cells (1.5×10^6 cells/well) grown in six-well plates were washed with PBS (1 mL × 3), harvested, incubated with PI (5 μM), and analyzed by using the FACSCalibur-HTS flow cytometer (BD Biosciences) (20 000 events per sample were acquired). The FL2 channel was used to assess intracellular PI uptake. Cell populations were analyzed using the FlowJo software (Tree Star).

Fluorescence Microscopy. A549 cells (1.5×10^6 cells/well) were incubated with and without **1** and **2** (20 μM) for 12 h. The media were then removed, and the cells were washed with additional media (2 mL × 2). After incubation of the cells with more media containing Hoechst 33258 (7.5 μM) and PI (5 μM), the nuclear regions were imaged using a fluorescence microscope. Fluorescence imaging experiments were performed using a Zeiss Axiovert 200M inverted epifluorscence microscope with a Hamamatsu EM-CCD digital camera C9100 and a MS200 XY Piezo Z stage (Applied Scientific Instruments, Inc.). An X-Cite 120 metal halide lamp (EXFO) was used as the light source. Zeiss standard filter set 49 was employed for imaging the nuclear region. The microscope was operated with Volocity software (version 6.01, Improvision). The exposure time for acquisition of fluorescence images was kept constant for each series of images at each channel.

Immunoblotting Analysis. A549 cells (1.5×10^6 cells/well) grown in six-well plates were incubated with **1** and **2** (concentrations, sub-μM) for 72 h at 37 °C. Cells were washed with PBS, scraped into SDS-PAGE loading buffer (64 mM Tris-HCl (pH 6.8)/9.6% glycerol/2% SDS/5% β-mercaptoethanol/0.01% Bromophenol Blue), and incubated at 95 °C for 10 min. Whole cell lysates were resolved by 4−20% sodium dodecyl sulfate polyacylamide gel electrophoresis (SDS-PAGE; 200 V for 25 min), followed by electro-transfer to polyvinylidene difluoride membrane (350 mA for 1 h). Membranes were blocked in 5% (w/v) non-fat milk in PBST (PBS/0.1% Tween 20) and incubated with the appropriate primary antibodies (Cell Signalling Technology and Santa Cruz). After incubation with horseradish peroxidase-conjugated secondary antibodies (Cell Signalling Technology), immuno complexes were detected with the ECL detection reagent (BioRad) and analyzed using an Alpha Innotech ChemiImager 5500 instrument fitted with a chemiluminescence filter.

Cell Cycle. In order to monitor the cell cycle, flow cytometry studies were carried out. A549 cells (1.5×10^6 cells/well) grown in six-well plates were incubated with and without the test compounds for 24, 48, and 72 h at 37 °C. Cells were harvested from adherent cultures by trypsinization and combined with all detached cells from the incubation medium to assess total cell viability. Following centrifugation at 1000 rpm for 5 min, cells were washed with PBS and then fixed with 70% ethanol in PBS. Fixed cells were collected by centrifugation at 2500 rpm for 3 min, washed with PBS, and centrifuged as before. Cellular pellets were resuspended in 50 μg/mL PI (Sigma) in PBS for nucleic acids staining and treated with 100 μg/mL RNaseA (Sigma). DNA content was measured on a FACSCalibur-HTS flow cytometer (BD Biosciences) using laser excitation at 488 nm, and 20 000 events per sample were acquired. Cell cycle profiles were analyzed using the ModFit software.

■ ASSOCIATED CONTENT

Ⓢ Supporting Information

Experimental techniques and data concerning biophysical and cellular studies. This material is available free of charge via the Internet at http://pubs.acs.org.

■ AUTHOR INFORMATION

Corresponding Author

*lippard@mit.edu

Notes

The authors declare no competing financial interest.

■ ACKNOWLEDGMENTS

This work is supported by the NCI under grant CA034992.

■ REFERENCES

(1) *Cancer Facts & Figures 2013*; American Cancer Society: Atlanta, GA, 2013.
(2) Fricker, S. P. *Dalton Trans.* **2007**, 4903.
(3) Kelland, L. *Nat. Rev. Cancer* **2007**, *7*, 573.
(4) Brabec, V.; Kasparkova, J. *Drug Resist. Updates* **2005**, *8*, 131.
(5) McWhinney, S. R.; Goldberg, R. M.; McLeod, H. L. *Mol. Cancer Ther.* **2009**, *8*, 10.
(6) Siddik, Z. H. *Oncogene* **2003**, *22*, 7265.
(7) Guo, Z. J.; Sadler, P. J. *Angew. Chem. Int. Ed.* **1999**, *38*, 1513.
(8) Lo, K. K.-W.; Zhang, K. Y.; Li, S. P.-Y. *Eur. J. Inorg. Chem.* **2011**, *2011*, 3551.
(9) Thorp-Greenwood, F. L.; Balasingham, R. G.; Coogan, M. P. *J. Organomet. Chem.* **2012**, *714*, 12.
(10) Leonidova, A.; Gasser, G. *ACS Chem. Biol.* **2014**, *9*, 2180.
(11) Ma, D.-L.; Che, C.-M.; Siu, F.-M.; Yang, M.; Wong, K.-Y. *Inorg. Chem.* **2007**, *46*, 740.
(12) Wang, W.; Yan, Y. K.; Andy Hor, T. S.; Vittal, J. J.; Wheaton, J. R.; Hall, I. H. *Polyhedron* **2002**, *21*, 1991.
(13) Yan, Y. K.; Cho, S. E.; Shaffer, K. A.; Rowell, J. E.; Barnes, B. J.; Hall, I. H. *Pharmazie* **2000**, *55*, 307.
(14) Zhang, J.; Vittal, J. J.; Henderson, W.; Wheaton, J. R.; Hall, I. H.; Hor, T. S. A.; Yan, Y. K. *J. Organomet. Chem.* **2002**, *650*, 123.
(15) Kitanovic, I.; Can, S.; Alborzinia, H.; Kitanovic, A.; Pierroz, V.; Leonidova, A.; Pinto, A.; Spingler, B.; Ferrari, S.; Molteni, R.; Steffen, A.; Metzler-Nolte, N.; Wölfl, S.; Gasser, G. *Chem.—Eur. J.* **2014**, *20*, 2496.
(16) Leonidova, A.; Pierroz, V.; Rubbiani, R.; Heier, J.; Ferrari, S.; Gasser, G. *Dalton Trans.* **2014**, *43*, 4287.
(17) Leonidova, A.; Pierroz, V.; Rubbiani, R.; Lan, Y.; Schmitz, A. G.; Kaech, A.; Sigel, R. K. O.; Ferrari, S.; Gasser, G. *Chem. Sci.* **2014**, *5*, 4044.
(18) Martinez-Lillo, J.; Mastropietro, T. F.; Lappano, R.; Madeo, A.; Alberto, M. E.; Russo, N.; Maggiolini, M.; De Munno, G. *Chem. Commun.* **2011**, *47*, 5283.
(19) Clarke, M. J.; Zhu, F.; Frasca, D. R. *Chem. Rev.* **1999**, *99*, 2511.
(20) Jakupec, M. A.; Galanski, M.; Arion, V. B.; Hartinger, C. G.; Keppler, B. K. *Dalton Trans.* **2008**, 183.

DOI: 10.1021/ja511978y
J. Am. Chem. Soc. 2015, 137, 2967−2974

(21) Dimitrov, N. V.; Eastland, G. W. In *Current Chemotherapy*; Siegenthaler, W., Luthy, R., Eds.; American Society of Microbiology: Washington, DC, 1978; Vol. 2.
(22) Shtemenko, N.; Collery, P.; Shtemenko, A. In *Metal Ions in Biology and Medicine*; Alpoim, M. C., Morais, P. V., Santos, M. A., Cristovao, A. J., Centeno, J. A., Collery, P., Eds.; John Libbey Eurotext: Paris, France, 2006; Vol. *9*, p 374.
(23) Shtemenko, N.; Collery, P.; Shtemenko, A. In *Metal Ions in Biology and Medicine*; Collery, P., Maymard, I., Thephanides, T., Khassanova, L., Collery, T., Eds.; John Libbey Eurotext: Paris, France, 2008; Vol. *10*, p 441.
(24) Shtemenko, A. G., Tretyak, S.; Shtemenko, N.; Randarevich, M. In *Metal Ions in Biology and Medicine*; Collery, P., Maymard, I., Thephanides, T., Khassanova, L., Collery, T., Eds.; John Libbey Eurotext: Paris, France, 2008; Vol. *10*, p 229.
(25) Shtemenko, N. I.; Zabitskaya, E. D.; Berzenina, O. V.; Yegorova, D. E.; Shtemenko, A. V. *Chem. Biodivers.* **2008**, *5*, 1660.
(26) Shtemenko, A. V.; Collery, P.; Shtemenko, N. I.; Domasevitch, K. V.; Zabitskaya, E. D.; Golichenko, A. A. *Dalton Trans.* **2009**, 5132.
(27) Shtemenko, N.; Collery, P.; Shtemenko, A. *Anticancer Res.* **2007**, *27*, 2487.
(28) Fischer, U.; Schulze-Osthoff, K. *Cell Death Differ.* **2005**, *12* (Suppl 1), 942.
(29) Hickman, J. A. *Cancer Metastasis Rev.* **1992**, *11*, 121.
(30) Jamieson, E. R.; Lippard, S. J. *Chem. Rev.* **1999**, *99*, 2467.
(31) Wang, D.; Lippard, S. J. *Nat. Rev. Drug Discovery* **2005**, *4*, 307.
(32) Cepero, V.; Garcia-Serrelde, B.; Moneo, V.; Blanco, F.; Gonzalez-Vadillo, A. M.; Alvarez-Valdes, A.; Navarro-Ranninger, C.; Carnero, A. *Clin. Trans. Oncol.* **2007**, *9*, 521.
(33) Ernst, R. J.; Komor, A. C.; Barton, J. K. *Biochemistry* **2011**, *50*, 10919.
(34) Han, W.; Li, L.; Qiu, S.; Lu, Q.; Pan, Q.; Gu, Y.; Luo, J.; Hu, X. *Mol. Cancer Ther.* **2007**, *6*, 1641.
(35) Vandenabeele, P.; Galluzzi, L.; Vanden Berghe, T.; Kroemer, G. *Nat. Rev. Mol. Cell Biol.* **2010**, *11*, 700.
(36) Pasparakis, M.; Vandenabeele, P. *Nature* **2015**, *517*, 311.
(37) Li, J.; McQuade, T.; Siemer, A. B.; Napetschnig, J.; Moriwaki, K.; Hsiao, Y. S.; Damko, E.; Moquin, D.; Walz, T.; McDermott, A.; Chan, F. K.; Wu, H. *Cell* **2012**, *150*, 339.
(38) Irrinki, K. M.; Mallilankaraman, K.; Thapa, R. J.; Chandramoorthy, H. C.; Smith, F. J.; Jog, N. R.; Gandhirajan, R. K.; Kelsen, S. G.; Houser, S. R.; May, M. J.; Balachandran, S.; Madesh, M. *Mol. Cell. Biol.* **2011**, *31*, 3745.
(39) Huang, C.; Luo, Y.; Zhao, J.; Yang, F.; Zhao, H.; Fan, W.; Ge, P. *PLoS One* **2013**, *8*, e66326.
(40) Longley, D. B.; Johnston, P. G. *J. Pathol.* **2005**, *205*, 275.
(41) Pommier, Y.; Sordet, O.; Antony, S.; Hayward, R. L.; Kohn, K. W. *Oncogene* **2004**, *23*, 2934.
(42) Simstein, R.; Burow, M.; Parker, A.; Weldon, C.; Beckman, B. *Exp. Biol. Med.* **2003**, *228*, 995.
(43) Reithofer, M. R.; Bytzek, A. K.; Valiahdi, S. M.; Kowol, C. R.; Groessl, M.; Hartinger, C. G.; Jakupec, M. A.; Galanski, M.; Keppler, B. K. *J. Inorg. Biochem.* **2011**, *105*, 46.
(44) Reithofer, M. R.; Schwarzinger, A.; Valiahdi, S. M.; Galanski, M.; Jakupec, M. A.; Keppler, B. K. *J. Inorg. Biochem.* **2008**, *102*, 2072.
(45) Suntharalingam, K.; Wilson, J. J.; Lin, W.; Lippard, S. J. *Metallomics* **2014**, *6*, 437.
(46) Galluzzi, L.; Senovilla, L.; Vitale, I.; Michels, J.; Martins, I.; Kepp, O.; Castedo, M.; Kroemer, G. *Oncogene* **2012**, *31*, 1869.
(47) Jiang, H.; Pritchard, J. R.; Williams, R. T.; Lauffenburger, D. A.; Hemann, M. T. *Nat. Chem. Biol.* **2011**, *7*, 92.
(48) Pritchard, J. R.; Bruno, P. M.; Gilbert, L. A.; Capron, K. L.; Lauffenburger, D. A.; Hemann, M. T. *Proc. Natl. Acad. Sci. U.S.A.* **2013**, *110*, E170.
(49) Pritchard, J. R.; Bruno, P. M.; Hemann, M. T.; Lauffenburger, D. A. *Mol. BioSyst.* **2013**, *9*, 1604.
(50) Slee, E. A.; Zhu, H.; Chow, S. C.; MacFarlane, M.; Nicholson, D. W.; Cohen, G. M. *Biochem. J.* **1996**, *315*, 21.
(51) Degterev, A.; Hitomi, J.; Germscheid, M.; Ch'en, I. L.; Korkina, O.; Teng, X.; Abbott, D.; Cuny, G. D.; Yuan, C.; Wagner, G.; Hedrick, S. M.; Gerber, S. A.; Lugovskoy, A.; Yuan, J. *Nat. Chem. Biol.* **2008**, *4*, 313.
(52) Degterev, A.; Huang, Z.; Boyce, M.; Li, Y.; Jagtap, P.; Mizushima, N.; Cuny, G. D.; Mitchison, T. J.; Moskowitz, M. A.; Yuan, J. *Nat. Chem. Biol.* **2005**, *1*, 112.
(53) Dodo, K.; Katoh, M.; Shimizu, T.; Takahashi, M.; Sodeoka, M. *Bioorg. Med. Chem. Lett.* **2005**, *15*, 3114.
(54) Feoktistova, M.; Geserick, P.; Kellert, B.; Dimitrova, D. P.; Langlais, C.; Hupe, M.; Cain, K.; MacFarlane, M.; Hacker, G.; Leverkus, M. *Mol. Cell* **2011**, *43*, 449.
(55) Tenev, T.; Bianchi, K.; Darding, M.; Broemer, M.; Langlais, C.; Wallberg, F.; Zachariou, A.; Lopez, J.; MacFarlane, M.; Cain, K.; Meier, P. *Mol. Cell* **2011**, *43*, 432.
(56) Wang, L.; Du, F.; Wang, X. *Cell* **2008**, *133*, 693.
(57) Cho, Y.; Challa, S.; Moquin, D.; Genga, R.; Ray, T. D.; Guildford, M.; Chan, F. K.-M. *Cell* **2009**, *137*, 1112.
(58) Davis, C. W.; Hawkins, B. J.; Ramasamy, S.; Irrinki, K. M.; Cameron, B. A.; Islam, K.; Daswani, V. P.; Doonan, P. J.; Manevich, Y.; Madesh, M. *Free Radic. Biol. Med.* **2010**, *48*, 306.
(59) Zhang, D.-W.; Shao, J.; Lin, J.; Zhang, N.; Lu, B.-J.; Lin, S.-C.; Dong, M.-Q.; Han, J. *Science* **2009**, *325*, 332.
(60) He, S.; Wang, L.; Miao, L.; Wang, T.; Du, F.; Zhao, L.; Wang, X. *Cell* **2009**, *137*, 1100.
(61) Temkin, V.; Huang, Q.; Liu, H.; Osada, H.; Pope, R. M. *Mol. Cell. Biol.* **2006**, *26*, 2215.
(62) Reers, M.; Smith, T. W.; Chen, L. B. *Biochemistry* **1991**, *30*, 4480.
(63) Smiley, S. T.; Reers, M.; Mottola-Hartshorn, C.; Lin, M.; Chen, A.; Smith, T. W.; Steele, G. D.; Chen, L. B. *Proc. Natl. Acad. Sci. U.S.A.* **1991**, *88*, 3671.
(64) Kaczmarek, A.; Vandenabeele, P.; Krysko, D. V. *Immunity* **2013**, *38*, 209.
(65) Sosna, J.; Voigt, S.; Mathieu, S.; Lange, A.; Thon, L.; Davarnia, P.; Herdegen, T.; Linkermann, A.; Rittger, A.; Chan, F. K.; Kabelitz, D.; Schutze, S.; Adam, D. *Cell. Mol. Life Sci.* **2014**, *71*, 331.
(66) Xu, X.; Chua, C. C.; Zhang, M.; Geng, D.; Liu, C.-F.; Hamdy, R. C.; Chua, B. H. L. *Brain Res.* **2010**, *1343*, 206.
(67) Latt, S. A.; Stetten, G. *J. Histochem. Cytochem.* **1976**, *24*, 24.
(68) Lecoeur, H. *Exp. Cell Res.* **2002**, *277*, 1.
(69) Schreiber, V.; Dantzer, F.; Ame, J.-C.; de Murcia, G. *Nat. Rev. Mol. Cell Biol.* **2006**, *7*, 517.
(70) Los, M.; Mozoluk, M.; Ferrari, D.; Stepczynska, A.; Stroh, C.; Renz, A.; Herceg, Z.; Wang, Z. Q.; Schulze-Osthoff, K. *Mol. Biol. Cell* **2002**, *13*, 978.
(71) Tu, H.-C.; Ren, D.; Wang, G. X.; Chen, D. Y.; Westergard, T. D.; Kim, H.; Sasagawa, S.; Hsieh, J. J.-D.; Cheng, E. H. *Proc. Natl. Acad. Sci. U.S.A.* **2009**, *106*, 1093.
(72) Greay, S. J.; Ireland, D. J.; Kissick, H. T.; Levy, A.; Beilharz, M. W.; Riley, T. V.; Carson, C. F. *Cancer Chemother. Pharmacol.* **2010**, *65*, 877.
(73) Sane, A. T.; Bertrand, R. *Cancer Res.* **1999**, *59*, 3565.
(74) Pabla, N.; Dong, G.; Jiang, M.; Huang, S.; Kumar, M. V.; Messing, R. O.; Dong, Z. *J. Clin. Invest.* **2011**, *121*, 2709.
(75) Zheng, Y.-R.; Suntharalingam, K.; Johnstone, T. C.; Yoo, H.; Lin, W.; Brooks, J. G.; Lippard, S. J. *J. Am. Chem. Soc.* **2014**, *136*, 8790.
(76) Erdlenbruch, B.; Nier, M.; Kern, W.; Hiddemann, W.; Pekrun, A.; Lakomek, M. *Eur. J. Clin. Pharmacol.* **2001**, *57*, 393.
(77) Mitsopoulou, C. A.; Dagas, C. *Bioinorg. Chem. Appl.* **2010**, 973742.
(78) Machura, B.; Świtlicka, A.; Wolff, M.; Kusz, J.; Kruszynski, R. *Polyhedron* **2009**, *28*, 3999.

DOI: 10.1021/ja511978y
J. Am. Chem. Soc. 2015, 137, 2967−2974